Stopping of hypervelocity clusters in solids

2011 New J. Phys. 13 113019

(http://iopscience.iop.org/1367-2630/13/11/113019)

New Journal of Physics
The open-access journal for physics

Stopping of hypervelocity clusters in solids

Christian Anders[1], **Eduardo M Bringa**[2], **Gerolf Ziegenhain**[1] **and Herbert M Urbassek**[1,3]

[1] Fachbereich Physik und Forschungszentrum OPTIMAS, Universität Kaiserslautern, Erwin-Schrödinger-Straße, D-67663 Kaiserslautern, Germany
[2] CONICET and Instituto de Ciencias Básicas, Universidad Nacional de Cuyo, Mendoza 5500, Argentina
E-mail: urbassek@rhrk.uni-kl.de

New Journal of Physics **13** (2011) 113019 (17pp)
Received 29 July 2011
Published 17 November 2011
Online at http://www.njp.org/
doi:10.1088/1367-2630/13/11/113019

Abstract. Using molecular-dynamics simulations, we study the processes underlying the stopping of energetic clusters upon impact in matter. We investigate self-bombardment of both a metallic (Cu) and a van-der-Waals bonded (frozen Ar) target. Clusters with sizes up to $N = 10^4$ atoms and with energies per atom of $E/N = 0.1$–$1600\,\mathrm{eV\,atom^{-1}}$ were studied. We find that the stopping force exerted on a cluster follows an $N^{2/3}$-dependence with cluster size N; thus large clusters experience less stopping than equi-velocity atoms. In the course of being stopped, the cluster is strongly deformed and attains a roughly pancake shape. Due to the cluster inertia, maximum deformation occurs later than the maximum stopping force. The time scale of projectile stopping is set by t_0, the time the cluster needs to cover its own diameter before impacting the target; it thus depends on both cluster size and velocity. The time when the cluster experiences its maximum stopping force is around $(0.7$–$0.8)t_0$. We find that the cluster is deformed with huge strain rates of around $1/2t_0$; this amounts to 10^{11}–$10^{13}\,\mathrm{s^{-1}}$ for the cases studied here.

[3] Author to whom any correspondence should be addressed.

Contents

1. Introduction

While the interaction of monatomic projectiles with solid surfaces has been investigated quite thoroughly in recent decades and a mature understanding has been reached, the physics of cluster–surface interaction contains more complex phenomena and both experimental and theoretical investigations are still under way. Such interactions occur in nature in the space environment where interplanetary or interstellar dust particles with sizes ranging down to nanometers interact with the surfaces of astronomical objects or with spacecraft [1, 2]. Further applications are found in the field of secondary ion mass spectrometry, where cluster projectiles are used to enhance the sputtering rate and the ionization efficiency of the emitted material [3–8]. Other applications include cluster deposition on surfaces [9], thin-film formation [10–15] or surface smoothing [16].

The basic quantity characterizing cluster–surface interaction is the stopping force exerted by the target on the cluster. While for a monatomic projectile the stopping force is an unambiguous function of the projectile velocity (for a given projectile and target species), the situation is not so clear-cut for a cluster projectile, since stopping is dependent on the shape of the cluster, and the shape changes during stopping. Figure 1 gives an example for the case of a 1 MeV $Cu_{10\,000}$ cluster. Ultimately, the cluster may fragment into smaller parts or even into its atomic constituents—in the latter case, stopping is simply the sum of individual atomic stopping forces. However, for not too weakly bound clusters, the *maximum* stopping force on a cluster is quite well defined. It occurs while the cluster is still penetrating through the surface and has still kept—more or less—its initial shape, before fragmentation sets in. It is on this maximum stopping force that this paper concentrates.

Recently, it was found that the stopping of a cluster composed of N atoms increases roughly $\propto N^{2/3}$, i.e. it depends on the cluster cross-sectional area rather than its volume [17, 18]. Hence, large clusters are stopped considerably less efficiently than N individual atoms of the same velocity. Other studies on cluster stopping are rare [19]. In this paper, we wish to explore the dependence on cluster energy and cluster size in a systematic way. While we stick to the case of self-bombardment, we study two widely different materials: Ar as a weakly bound material and

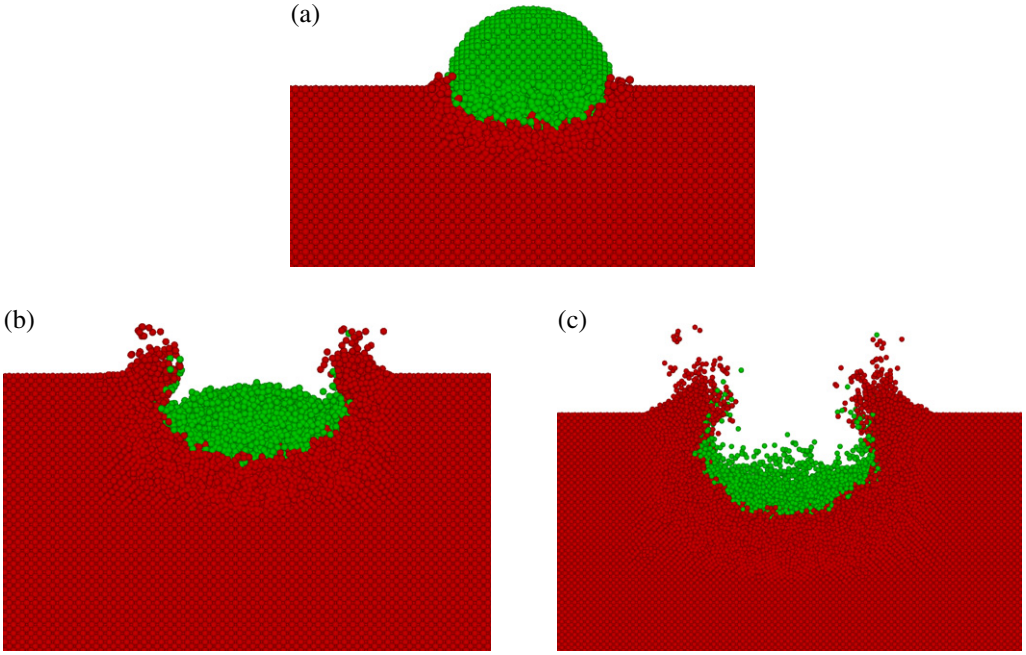

Figure 1. 1 MeV $Cu_{10\,000}$ cluster (green) impinging on a (100) Cu target crystal (red) at various times after impact, i.e. after the cluster started interacting with the target. (a) $t = 0.21$ ps, close to the time of the maximum stopping force. (b) $t = 0.43$ ps, close to the time of maximum deformation. (c) $t = 0.73$ ps, after cluster fragmentation set in. The target width displayed amounts to 16.6 nm.

Cu as a prototypical metal. In addition, we compare to previous results obtained for Au cluster impact of an Ar target [20]. We shall demonstrate—for cluster velocities in the range of up to several tens of km s^{-1} and cluster sizes $N \leqslant 10^4$—that the stopping force on a cluster is quite well defined and obeys a simple power-law behavior on projectile energy and size. Projectile deformation—as well as the associated strain rate—are also studied, since it determines if and how long the projectile will stay unfragmented—otherwise different physics will apply.

2. Method

2.1. Systems

We investigate the impact of clusters on an amorphous Ar and a crystalline Cu (100) target. The Ar–Ar interaction potential is a pair potential of the Lennard–Jones form [21, 22], splined to the KrC potential [23] and valid for close Ar–Ar encounters. The Cu–Cu interaction potential uses a many-body potential [24, 25] with a Ziegler–Biersack–Littmark pair interaction [26] for high-energy encounters. We note that in the energy range of a few eV to a few hundreds of eV relevant for our work, the interatomic interaction potential is not well known; the results obtained by the above-mentioned potentials may hence not be quantitatively realistic in all cases. Since, however, we shall see good qualitative agreement between the results obtained for Ar and Cu—with their very different bonding characteristics and interaction potentials—we can be confident that our qualitative conclusions are reliable. The targets have free surfaces,

which were relaxed before starting bombardment, while the lateral and bottom surfaces employ damped boundary conditions [27].

Spherical Ar and Cu clusters were prepared by cutting them out from the bulk specimens and relaxing their shape. For a frozen amorphous Ar target, we investigate cluster sizes of 13, 100, 1000 and 10 000 atoms and total impact energies of 0.1–4 keV, and for $Ar_{10\,000}$, up to 200 keV. For a crystalline Cu target with the (100) surface the cluster sizes are 43, 100, 1000 and 10 000 atoms with total impact energies of 1–3000 keV. Thus the energy per atom was varied in the range of $E/N = 0.1$–80 eV for Ar and $E/N = 5$–1600 eV for Cu. We note that there are limitations to the energy and size of the simulated clusters. If we consider a large cluster, which also has a large E/N, the total energy deposited in a small volume of the target could take the material to pressures and temperatures where classical molecular dynamics and the potentials we are considering are no longer valid. For metals, these conditions typically mean temperatures and pressures beyond a few eV and a fraction of a TPa, respectively.

The projectile is started downwards in the $-x$-direction outside the interaction zone of the target. The molecular-dynamics simulation is performed until the (maximum) stopping force and projectile deformation have been determined. This occurs within roughly 1 ps for Cu and 4 ps for Ar; hence our simulations are considerably shorter than those needed to simulate the projectile range, the induced sputtering or the crater formation [28–30]. We disregard electronic stopping in the simulation, since the projectile velocities are quite small; our results thus exclusively describe the nuclear stopping of the projectile.

For the simulation, both our own molecular-dynamics code [20, 24] and the public-domain code LAMMPS (http://lammps.sandia.gov/) have been employed. The results for each cluster size and impact energy have been averaged over several (typically 5) events, in which different cluster impact points and different target specimens have been used, in order to generate sufficient statistics. The target sizes have been varied between 7×10^4 and 7×10^6 atoms, depending on cluster energy and size. As an example, for simulations of 4 keV Ar_{1000} impact we employed a target consisting of 270 000 atoms; this guaranteed that the cluster stayed sufficiently far away from the sides and the bottom of the simulation target for the result to remain reliable during the time of cluster stopping. We made sure that within the simulation time the clusters did stay sufficiently far away from the bottom and lateral target boundaries in order not to affect our results.

2.2. Stopping

Figure 2 shows how the stopping force is determined from the deceleration of the projectile center-of-mass trajectory. For this purpose the x-component of the projectile center-of-mass velocity, v, is plotted as a function of time. Using a tangent, we determine the maximum slope of $v(x)$, i.e. the maximum acceleration and hence stopping force. As figure 2 demonstrates, the tangent fits the velocity quite well over a finite time interval. This allows us to obtain the stopping force via

$$\frac{\mathrm{d}E}{\mathrm{d}x} = Mv\frac{\mathrm{d}v}{\mathrm{d}x} = M\frac{\mathrm{d}v}{\mathrm{d}t} = Ma = Nma. \tag{1}$$

Here, M denotes the total mass of the projectile, m the mass of an individual projectile atom and a the center-of-mass projectile acceleration. Note that due to our choice of the coordinate system, $x < 0$ inside the target; hence $v < 0$, while a and $\mathrm{d}E/\mathrm{d}x > 0$.

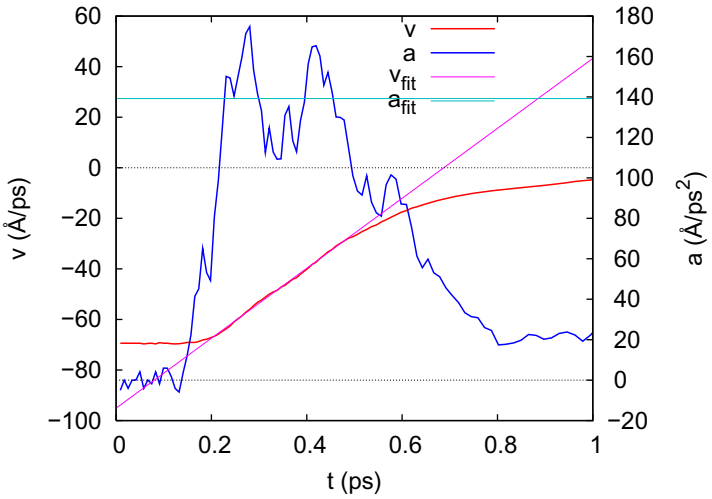

Figure 2. Velocity v and deceleration a of an Ar_{100} cluster impacting at 1 keV on an amorphous Ar target. Both observables are fitted to straight lines—v_{fit} and a_{fit}, respectively—in the interval from 0.22 to 0.48 ps.

In molecular-dynamics the deceleration a could also be directly obtained from the simulation data; however, as figure 2 demonstrates, the data are too noisy. Our approach to determine the (maximum) stopping force thus agrees with the procedure used in [20].

We note that this method will not work if the cluster does not interact collectively with the target, but rather individual collisions between cluster and target atoms dominate the stopping. This shows up in the data as strong fluctuations in the stopping force, where the peaks are correlated with individual atomic collisions. This occurs for small cluster sizes (cf the Ar_{13} cluster data of figure 12(a) below) and for high impact energies (cf the 1 MeV $Cu_{10\,000}$ data of figure 11 below). Velocity data showing stronger fluctuations can still be averaged by a line fit over a finite interval, but this introduces some arbitrariness into the procedure. Furthermore, in the chosen deceleration time interval, in which the fit is performed, the projectile should at least penetrate about a lattice constant, in order to average out the discrete target atomic structure.

2.3. Deformation

We define the deformation (*strain*) of the projectile by the change of its relative height. Since the projectile is quickly deformed and assumes a complex shape, we measure its vertical elongation $d(t)$ as the standard deviation of the x-coordinates of the atomic positions

$$d = \sqrt{20}\sqrt{\sum_{i=1}^{N}(x_i - \bar{x})^2/N}, \tag{2}$$

where $\bar{x}$ denotes the center-of-mass coordinate of the cluster. The factor $\sqrt{20}$ has been introduced in equation (2) to make d equal to the diameter of a homogeneous sphere. The deformation or strain of the cluster is then defined as d/d_0, where d_0 is the initial cluster diameter. This allows us to calculate the (time-dependent) strain rate as

$$\eta(t) = -\frac{1}{d_0}\frac{\mathrm{d}d}{\mathrm{d}t}. \tag{3}$$

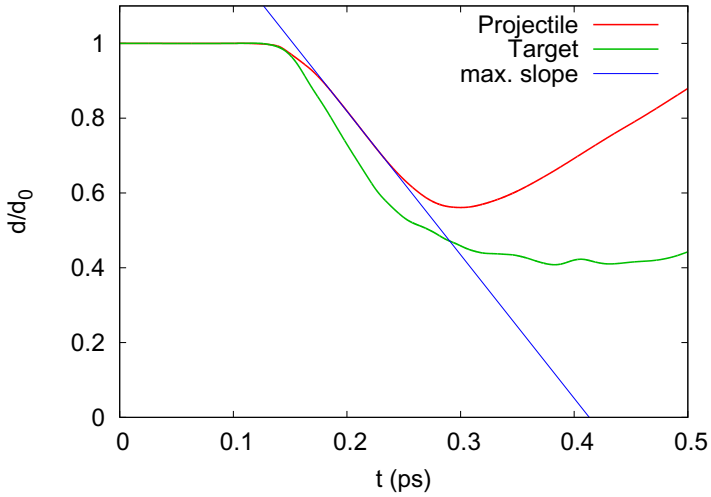

Figure 3. Temporal evolution of the relative projectile and target deformations perpendicular to the target surface for a 60 keV Cu_{1000} cluster impact on a Cu target. The straight line shows the maximum slope of the projectile deformation, which is used to identify the projectile strain rate. The artificial minimum in the cluster deformation is due to the onset of projectile fragmentation, as in figure 1(c).

In the following, we shall denote by η the *maximum* of the time-dependent strain rate, and denote it simply as the strain rate. Similar to the measurement of the stopping force, this maximum strain rate is determined by the tangent of the maximum slope to the deformation curve, cf figure 3. Note that in that plot, the projectile deformation appears to recover again, as if the projectile re-expanded; this is of course only a sign of cluster fragmentation. In particular at the cluster edges, friction dissolves the cluster, until the cluster finally has a crescent, rather than a lens-like, shape, cf figure 1.

Analogously, we could determine the strain and the strain rate in the target, which then of course depend strongly on the position inside the target where it is measured. The target strain data have been obtained by considering the deformation of an initially cuboid volume (lateral size 7 Å, height 18 Å) immediately below the projectile impact point. We note that for the projectile the deformation is also position dependent: figure 1 demonstrates that initially the lower part of the cluster experiences strongest compression, while the upper part is still unaffected; at later times, the projectile atoms at the cluster periphery, where lateral friction forces are maximum, display larger vertical variation than in the center. As a consequence, our 'global' detectors for projectile deformation and strain rate are useful only in the initial part of the stopping process. In particular, as soon as the cluster starts fragmenting or evaporating or its atoms become mixed into the target material, our definitions of deformation and strain rate lose their meaning. This will occur, however, only after the time of maximum deformation; hence our results, obtained before that time, remain valid. We also note that our definition of strain should not be confused with measures of uniaxial strain in systems constrained laterally, as in most shock wave simulations [31]. In our case the projectile does expand laterally, and the total volumetric strain of the projectile is typically below 25%, ensuring that we are still within a region of the phase diagram where classical molecular-dynamics works.

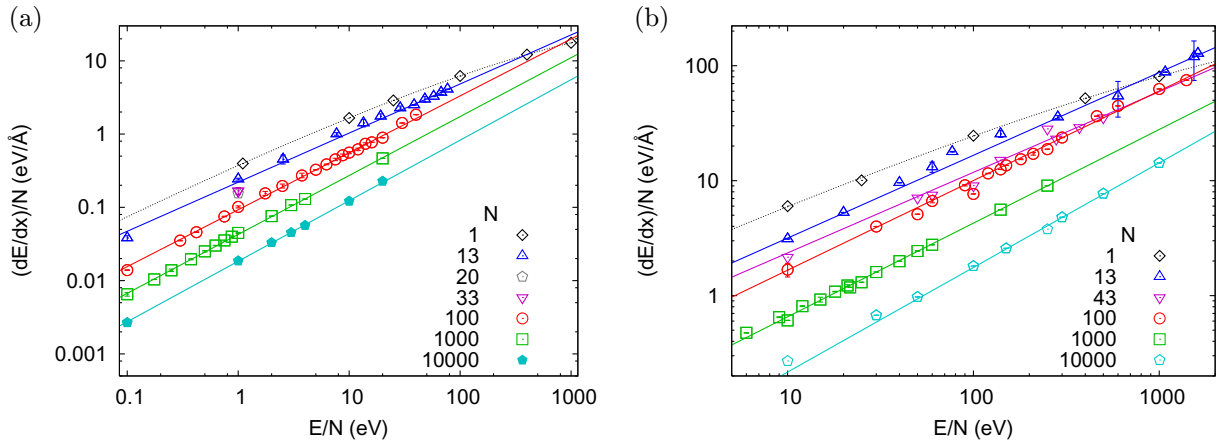

Figure 4. The stopping force per atom $(1/N)(\mathrm{d}E/\mathrm{d}x)$ of Ar clusters impacting an amorphous Ar target (a) and of Cu clusters impacting a Cu (100) surface (b). E is the total cluster impact energy and N denotes the number of cluster atoms. The cluster stopping is determined by our molecular-dynamics simulations, while the monomer stopping is computed by SRIM [26, 32].

3. Results

3.1. Stopping force

Figure 4 shows the dependence of the stopping force per projectile atom, $(1/N)(\mathrm{d}E/\mathrm{d}x)$, as a function of the cluster energy per atom, E/N, for Ar (a) and Cu (b). The figure demonstrates that larger clusters with the same E/N suffer less stopping than small clusters; a similar result for the Au→Ar system has previously been published [20]. The reason for this is the so-called clearing-the-way effect [33–36]: only the front atoms of the cluster interact with target atoms and feel the stopping force, while the remainder of the cluster keeps pushing forward. Since these front atoms hence have the task of 'clearing the way' for the remainder of the cluster, this phenomenon gave the effect its name.

The reduction in cluster stopping becomes even more noticeable if the cluster stopping data are normalized to the monomer stopping force. Figure 5 presents these reduced data for the Cu system; the data for the Ar system behave analogously.

In the range of energies investigated here, the stopping force per atom follows a power law with energy (cf figure 4), which may be parameterized as

$$\frac{1}{N}\frac{\mathrm{d}E}{\mathrm{d}x} = A(N)\left(\frac{E}{[\mathrm{eV}]}\right)^{\alpha(N)}. \tag{4}$$

The exponent α and prefactor A depend on cluster size N. These quantities are shown in figure 6. The monomer stopping follows a power law close to $E^{0.6}$. It is well known that stopping increases less than linearly for realistic repulsive interaction potentials at the small projectile energies considered here [37]. With increasing cluster size, the energy dependence becomes linear. Such a linear dependence is characteristic of the so-called 'hard-sphere' scattering (billiard balls) where particles interact with hard i.e. arbitrarily steep interaction potentials. To our knowledge, no theoretical argument exists regarding why the interaction of a cluster with

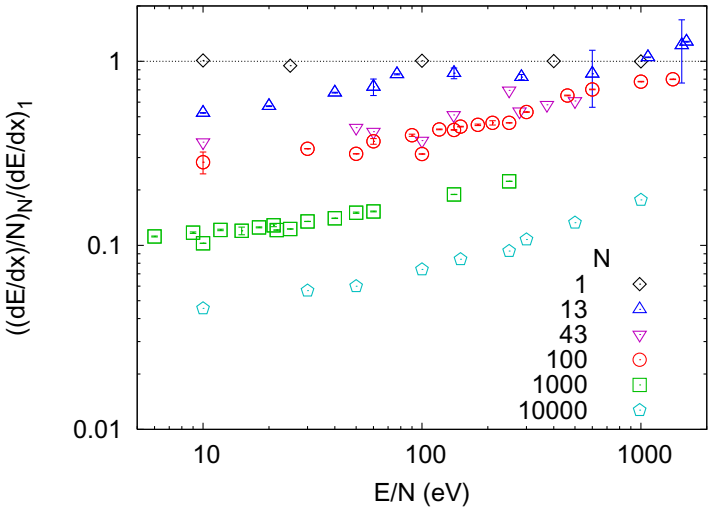

Figure 5. Stopping force per atom of Cu clusters, cf figure 4(b), normalized to that of a Cu atom.

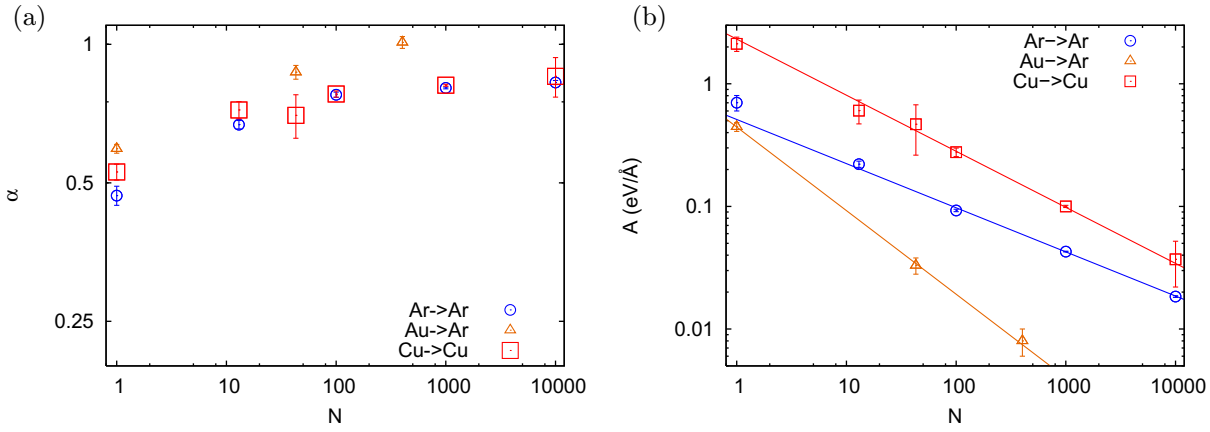

Figure 6. Exponent α (a) and prefactor A (b) of the power-law fit, equation (4), of the stopping force per atom, figure 4, as a function of cluster size N. Data on stopping of Au clusters in Ar [20] have been added.

a solid can be described by an energy-proportional stopping for large cluster sizes. We note, however, that the size dependence of stopping appears to be quite similar for the three systems included in this plot.

The clearing-the-way effect of larger clusters becomes visible in the prefactor A (figure 6), which decreases strongly with increasing cluster size. The figure shows that not only the properties of the target material (Cu versus Ar), but also those of the cluster itself (compare Au and Ar projectiles for the same Ar target), determine the prefactor.

Even more interesting is the analysis of the dependence of the cluster stopping (for constant E/N) on the cluster size (figure 7). This plot is a rearrangement of the data displayed in figure 6 (big symbols) or has been interpolated (small symbols) with the help of the fit lines in this plot when no simulations for the desired energy were available. The general trend for all impact energies is that large clusters suffer less stopping, as was already apparent in the

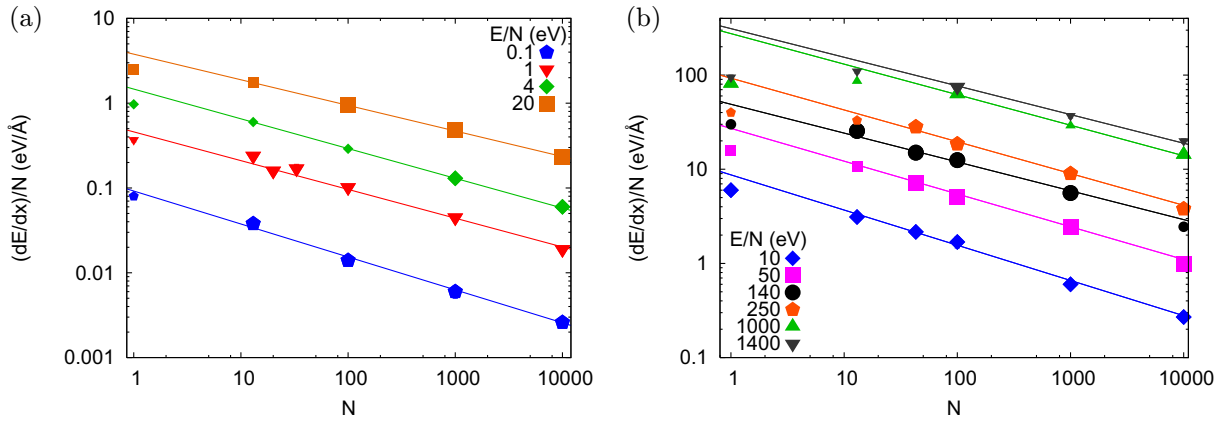

Figure 7. Dependence of the stopping force per atom $(1/N)(\mathrm{d}E/\mathrm{d}x)$ of Ar clusters impacting an amorphous Ar target (a) and of Cu clusters impacting a Cu (100) surface (b) on cluster size N.

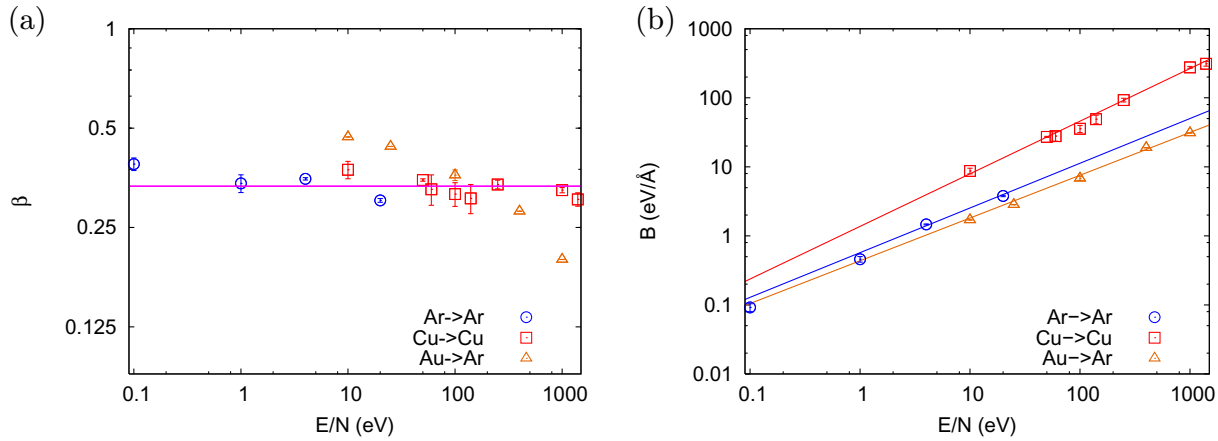

Figure 8. Exponent β (a) and prefactor B (b) of the power-law fit, equation (5), of the stopping force per atom (figure 7), as a function of cluster impact energy per atom, E/N. The line $\beta = 1/3$ in (a) is to guide the eye. Data on stopping of Au clusters in Ar [20] have been added.

cluster size dependence of the prefactor A in the fitting functions in figure 6 for the energy dependence.

The power-law dependence on size N seen in figure 7 suggests a fit of the form

$$\frac{1}{N}\frac{\mathrm{d}E}{\mathrm{d}x} = B(E/N)N^{-\beta(E/N)}. \tag{5}$$

Here, both the exponent β and prefactor B may depend on the energy per atom (and hence velocity) of the cluster; they are displayed in figure 8. Our data are compatible with a constant value of $\beta = 1/3$; a closer look shows that β may decrease slightly with E/N. This trend of a decreasing value of β is most pronounced for the Au→Ar system [20]. From a theoretical point of view, we expect that, for high E/N, the exponent approaches $\beta \to 0$, since for extremely high velocities we expect no size effect: every atom interacts more or less individually with the

target. The clearing-the-way effect becomes effective at our low velocities, where the exponent is compatible with a constant value of $\beta = 1/3$.

Note that a value of $\beta = 1/3$ has been postulated in an earlier work [17], combining experimental and simulational investigations on the impact of small Ag clusters on graphite. This value of β is equivalent to a total cluster stopping $\mathrm{d}E/\mathrm{d}x \propto N^{2/3}$ and hence amounts to the stopping being proportional to the cluster cross-sectional area.

The prefactor B (figure 8(b)) shows an increase with impact energy, which can be described by the power law $B(x) \propto x^{\tau}$. Here the exponent assumes constant values with $\tau = 0.65 \pm 0.05$ (0.76 ± 0.02) for the Ar→Ar (Cu → Cu) system and 0.62 ± 0.04 for Au→Ar.

It is hence tempting to attempt a joint power-law fit of the entire dependence of the stopping force per atom as a function of E and N via

$$\frac{1}{N}\frac{\mathrm{d}E}{\mathrm{d}x} = c\left(\frac{E}{[\mathrm{eV}]}\right)^{\alpha'} N^{-\beta'}. \tag{6}$$

Such a three-parameter fit of course has larger error bars than the fits (4) and (5) described above, in particular since the exponents have now to be assumed constant. We obtain $c = 0.39 \pm 0.03\,\mathrm{eV\,Å^{-1}}$, $\alpha' = 0.822 \pm 0.004$, $\beta' = 0.331 \pm 0.008$ for Ar→Ar, and $c = 1.12 \pm 0.08\,\mathrm{eV\,Å^{-1}}$, $\alpha' = 0.79 \pm 0.01$, $\beta' = 0.345 \pm 0.005$ for Cu → Cu.

The system Au→Ar cannot satisfactorily be fitted to equation (6), since the exponent of N shows a significant dependence on energy [20]. We assume that the reason is that the penetration and stopping of the heavy Au clusters in the weakly bonded Ar target constitute rather a special case of stopping: it constitutes the prototypical case of a hard and heavy projectile impacting a light and soft target [18, 20, 29].

3.2. Time of maximum stopping

For a monoatomic projectile (at energies below the stopping power maximum, as is the case in the present study), the stopping force is immediately maximum when it enters the target. This is different for a cluster, which needs some time to fully enter it; hence, the stopping force smoothly builds up, until the cluster is fully merged into the target, and then decreases again. Our procedure to measure the maximum stopping force on the projectile (cf section 2.2 and figure 2) also allows us to determine the time t_{stop} at which this maximum force is exerted.

Figure 9 shows how the time of the maximum stopping force depends on projectile energy E for different projectile sizes N. The data demonstrate that the time of maximum stopping increases with the cluster size and decreases with the impact energy. The data show a power-law dependence on E/N or equivalently on velocity v. We quantify this by introducing the time

$$t_0 = \frac{2R}{v}, \tag{7}$$

which a cluster of undecelerated velocity v needs to cover a distance equal to its diameter $2R$, where the radius R is given by

$$R = \left(\frac{3}{4\pi} N\Omega\right)^{1/3}. \tag{8}$$

Thus the time t_0 is an estimate of the time needed to fully embed the cluster in the target. Here, Ω is the atomic volume of the target material, $\Omega = 11.8$ and $36.1\,\mathrm{Å^3}$ for Cu and Ar, respectively.

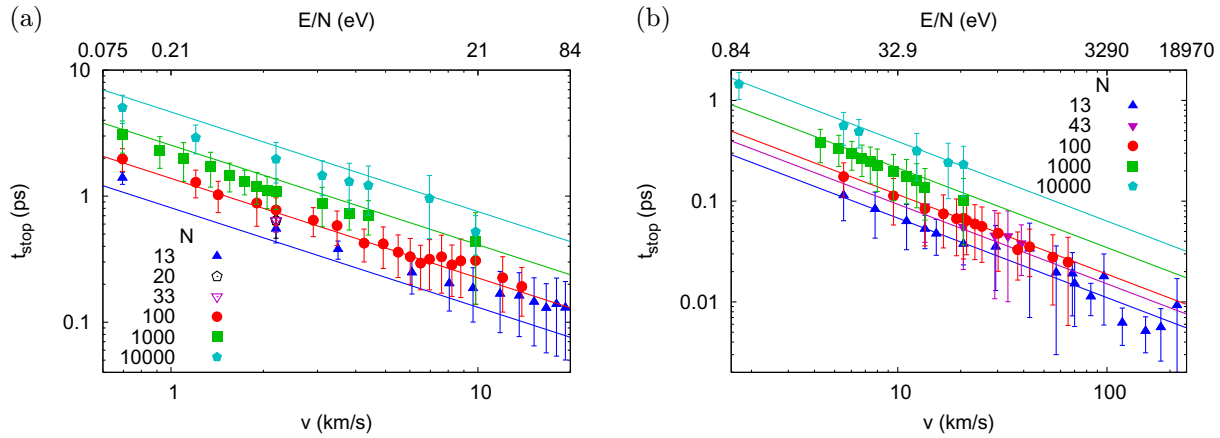

Figure 9. Time t_{stop} when stopping is maximum for Ar (a) and Cu clusters (b). The time is set to 0 when the cluster first starts interacting with the target. The bars are not error bars, but indicate the time intervals that have been used to determine the (maximum) stopping force (fit intervals used in figure 3). Lines: fit to equation (10).

In a simple model, the stopping time is proportional to t_0,

$$t_{\mathrm{stop}} = \epsilon t_0. \tag{9}$$

A fit to this law (not displayed here) gives values of $\epsilon = 0.71$ and 0.84 for Ar and Cu, respectively. This result hence shows that stopping becomes maximum within approximately the time t_0 the cluster needs to be fully embedded in the target.

We note, however, that the inverse velocity proportionality of equation (9) is not the optimum description of the data, and a slightly better fit can be obtained with

$$t_{\mathrm{stop}} = \epsilon' \left(\frac{t_0}{[\mathrm{ps}]} \right)^{\zeta}, \tag{10}$$

with $\epsilon' = 0.86$ (0.56) ps for Ar (Cu) and $\zeta = 0.79$ in both cases. The fit describes the Cu data satisfactorily; for Ar the deviations are larger and N-dependent fit parameters would be required for an improved fit.

We also include in figure 9 the lengths of the intervals during which the stopping force is roughly constant at its maximum value. This interval corresponds to the interval of time in figure 2, which was used for calculating the stopping force from the molecular dynamics data. These data demonstrate that our fit intervals are as a rule sufficiently long to base a reliable fit on them.

3.3. Deformation time

Besides the time of maximum stopping, the time of maximum cluster deformation is also relevant for describing the fate of a cluster after impact. If the cluster disintegrates before the time of maximum stopping, it is not stopped as an entity and its stopping is governed by the behavior of its constituents. We estimate the time of maximum deformation, t_{def}, by considering the procedure outlined in section 2.3 and figure 3. Our data for t_{def} are collected in figure 10.

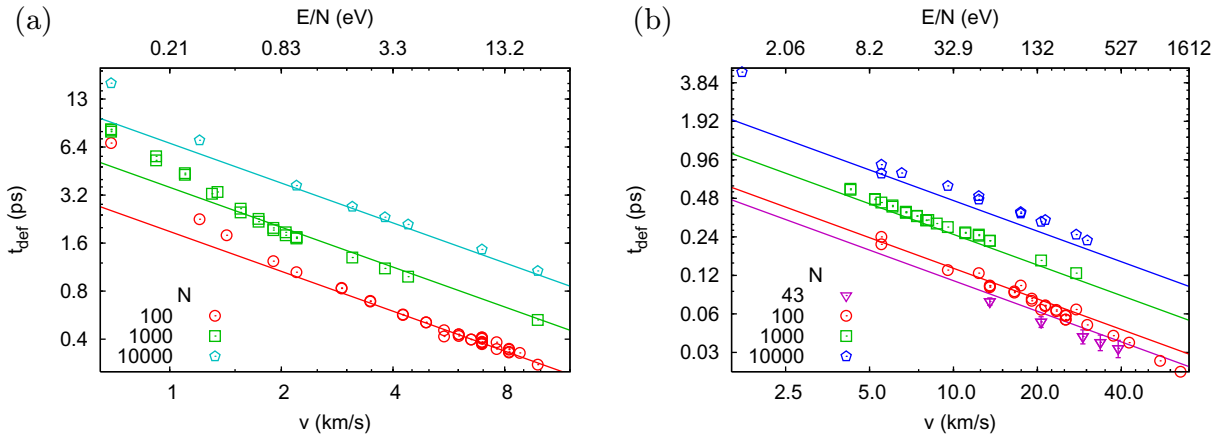

Figure 10. Time of maximum deformation, t_{def}, for Ar (a) and Cu (b) clusters. The time is set to 0 when the cluster first starts interacting with the target. Lines are a fit to equation (10).

Similarly to the time of maximum stopping (figure 9), the time of maximum deformation also exhibits a power-law dependence with velocity $\propto v^{-\beta}$, with powers $\beta = 0.80$–0.85 for both Ar and Cu. For impact velocities below the speed of sound in Ar, $v_{\mathrm{sound}} = 1.23\,\mathrm{km\,s^{-1}}$, the dependence becomes steeper, $\beta \cong 1.35$; this is a different stopping regime outside the *hypervelocity* impact region considered in this paper and will not be discussed here. Note that for Cu we did not attempt subsonic impacts ($v_{\mathrm{sound}} = 4.0\,\mathrm{km\,s^{-1}}$) except for the $\mathrm{Cu}_{10\,000}$ cluster, since at these velocities the cluster penetrates too little; this data point also shows an increased deformation time.

In the light of the discussion of the maximum stopping time, we attempt a simple fit based on an inverse velocity proportionality, as in equation (9). Our fit results in values of $\epsilon = 1.1$ and 0.95 for Ar and Cu, respectively. This shows that maximum deformation occurs only after maximum stopping; the time delay is of the order of (20–50)%. An (improved) power-law fit in the spirit of equation (10) yields $\epsilon' = 1.08$ (0.68) ps and $\zeta = 0.83$ (0.79) for Ar (Cu).

In figure 11, we analyze in detail the time dependence of stopping and deformation of the 1 MeV $\mathrm{Cu}_{10\,000}$ cluster, which has already provided the snapshots of figure 1. Note that stopping exhibits a rather broad maximum centered around 0.21 ps. The sharp spikes seen in the earlier part of the stopping process are due to individual cluster–atom encounters with target atoms; at these high speeds, the cluster is not initially stopped continuously, but rather by collisions of individual atoms at the cluster front. Deformation, however, shows a smooth behavior with a maximum around 0.4 ps, definitely later than maximum cluster stopping.

In this figure, we also added the internal cluster potential energy. It quickly rises with cluster stopping and shows a pronounced maximum at around 0.3 ps, after which it again rather quickly declines. The quick rise is due to the huge cluster compression during the early part of stopping, cf figure 1(a). The decline then is caused by the lateral cluster re-expansion. Note that the maximum potential energy of the cluster (65 keV) corresponds to 6.5 eV atom^{-1}; this value is considerably above the cohesive energy of Cu (3.54 eV) and already indicates the final fate of this collision: cluster fragmentation.

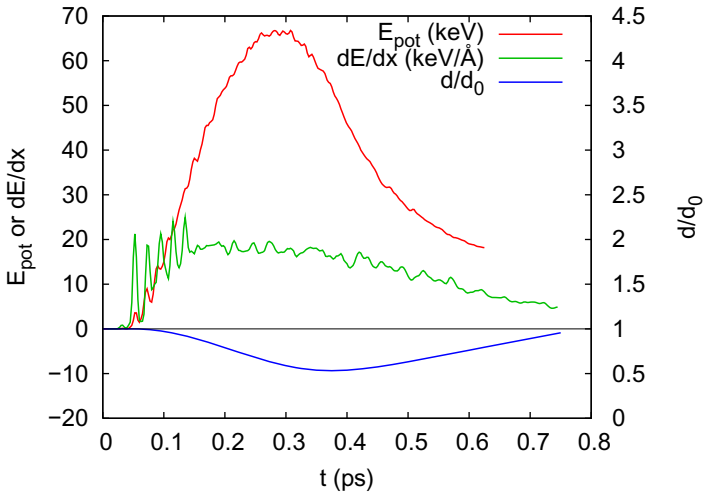

Figure 11. Time dependence of stopping of the $Cu_{10\,000}$ cluster of figure 1. Relative deformation d/d_0 (right abscissa), stopping force $\mathrm{d}E/\mathrm{d}x$ as determined from the cluster deceleration and potential energy E_{pot} of the projectile. E_{pot} has been set to 0 for the initial cluster.

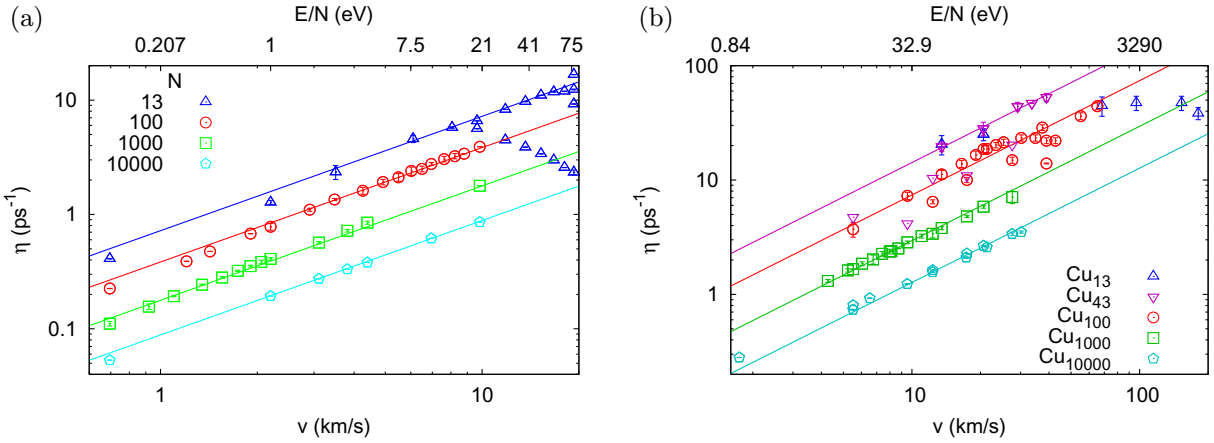

Figure 12. Strain rate η versus impact velocity v for Ar_N clusters impacting an Ar target (a) and for Cu_N clusters impacting a Cu target (b). Lines: linear fits, equation (11).

3.4. Strain rate

Strain rate estimates would be extremely useful for cluster bombardment. It is well known that plastic deformation can change dramatically with strain rate [38]. In addition, Insepov *et al* [39] proposed to use cluster impacts to estimate hardness and strength at the nanoscale, but many constitutive models imply that the strength is strongly strain rate dependent [40].

We calculate the projectile strain rate as the *maximum* rate with which the projectile height changes during the cluster stopping process; see section 2.3 and figure 3. We assemble our data for both Ar and Cu cluster stopping in figure 12. The data obey a simple scaling,

$$\eta = \gamma v. \tag{11}$$

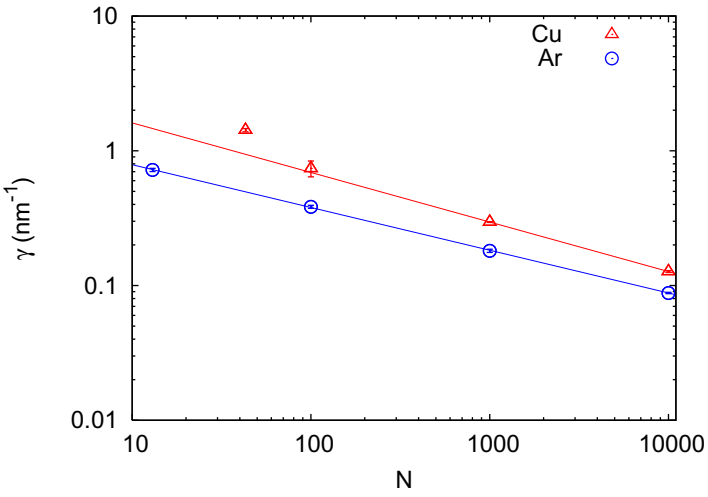

Figure 13. Strain rate slope $\gamma = \mathrm{d}\eta/\mathrm{d}v$ versus cluster size N for Ar and Cu. Fits to equation (14), see text.

This simple velocity proportionality may be rationalized as follows. During the time t_0, equation (7), which the projectile needs to become fully immersed into the target, it suffers a relative height change (deformation) of δ; as figure 3 shows, δ is about 0.5. Then the strain rate can be estimated as

$$\eta = \frac{\delta}{t_0} = \frac{\delta}{2R} v. \tag{12}$$

This gives us a value and a size dependence for the strain-rate coefficient γ as

$$\gamma = \frac{\delta}{2}\left(\frac{3}{4\pi}\frac{1}{N\Omega}\right)^{1/3}. \tag{13}$$

Figure 13 shows that the strain-rate slope γ as extracted from figure 12 decreases with increasing cluster size from 2 to 0.1 nm^{-1}. The power-law dependences

$$\gamma = \gamma_0 N^{-\xi} \tag{14}$$

included in this figure have been fitted to the data with exponents $\xi = 0.32$ and 0.37 for Ar and Cu, respectively; these values are in good agreement with the prediction $\xi = 0.33$, equation (13).

Also, the values of the prefactors $\gamma_0 = 1.63$ and 3.8 nm^{-1} obtained from the fit to the Ar and Cu data agree in their order of magnitude well with the values obtained from equation (13), which amount to 1.8δ (2.4δ) nm^{-1}. This model also explains why Cu cluster impact induces a higher strain rate than Ar; it is mainly due to the tighter packing of Cu atoms as compared to Ar atoms, i.e. to the atomic volume Ω appearing in equation (13).

The time $1/\eta = t_0/\delta \cong 2t_0$ is a rough measure of the time until complete cluster deformation and ensuing fragmentation; it agrees nicely with the quantitative data given in section 3.3. It estimates the maximum time within which the cluster can be treated as a slowing down sphere; after that time—at the latest—cluster deformation and fragmentation must be taken into account. These processes will strongly influence the further slowing down and penetration behavior of the cluster.

Figure 12 presents an irregular behavior for the small cluster sizes, $N < 100$; in particular, the data for $N = 13$ show artifacts for Ar clusters in the form of a 'bifurcation' of the data

for high projectile velocities. We studied these simulations in detail and found the following reason. For these small clusters, the exact impact position is important to determine the cluster fate: while for some impact points, the cluster atoms can penetrate deeper into the target, for others they are strongly decelerated by collisions with surface atoms. As soon as cluster atoms are scattered back from the target, our deformation detector measures an effective vertical 'elongation' of the cluster and hence a reduced strain. We consider this to be an artifact of our deformation and strain detector, which affects the evaluation of small clusters. While we are interested mainly in the effects of larger clusters ($N \geqslant 100$), we also showed our results for smaller clusters to point out the range of validity of our detector.

It is reassuring to find out that extrapolation of our strain rate results to macroscopic clusters leads to strain rates of $\sim 10^5\ \mathrm{s}^{-1}$, as expected from existing experiments and continuum-scale simulations [41, 42].

The immense strain rates found in these impacts can be achieved in laser-induced shock experiments carried out at large-scale laser facilities [38]. Such experiments are used to take materials to extreme conditions within their phase diagram, and achieve new phases and microstructures. Nanometer cluster bombardment could offer an alternative, when the desired effects need to be restricted to the surface, or could be used for exploring new materials-modification techniques based on transient effects.

4. Conclusions

We studied self-bombardment into two widely differing media, a frozen gas (Ar) and a metal (Cu). In addition, we made comparisons with previous stopping simulations of Au clusters impacting an Ar target. For a projectile exceeding $N \gtrsim 100$ atoms our results on projectile stopping and deformation show only small fluctuations caused by the atomistic nature of the projectile and target and appear reliable. We find the following.

(i) The stopping force exerted on a cluster follows in good approximation a $N^{2/3}$ dependence on cluster size N, i.e. it is proportional to the cross-sectional cluster area. The stopping force per atom of a cluster is thus smaller than that for a single atom with the same velocity. The physical reason for this is the so-called *clearing-the-way* effect [33–36], according to which only the front atoms of the cluster interact with target atoms and feel the stopping force, while the remainder of the cluster keeps pushing forward.

(ii) Our results on cluster stopping are qualitatively similar for the self-impact of Cu and Ar targets, indicating the universality of these results for self-impact. However, we find a slightly different behavior for Au clusters impinging on an Ar target; here, at high impact energies, the stopping force per atom tends to approach that of single atoms at the same velocity. Hence some caution must be used when extrapolating our results to systems where the cluster and the target consist of very different materials.

(iii) At the same velocity, large clusters suffer a stopping force proportional to the cluster energy E, even at velocities where individual atoms are stopped rather like $E^{0.6}$, as given by the interatomic forces.

(iv) In the course of being stopped, the cluster is strongly deformed and attains a roughly pancake shape. Due to the cluster inertia, maximum deformation occurs later than maximum stopping. After maximum compression, cluster fragmentation sets in, starting at the cluster periphery.

(v) The time scale of projectile stopping is given by t_0, equation (7), the time the cluster needs to cover its own diameter. The time when the cluster experiences the maximum stopping force is around $(0.7–0.8)t_0$; the time when its deformation along the impact direction is maximum occurs later.

(vi) Cluster deformation occurs with strain rates of approximately $1/2t_0$. For the clusters studied here this amounts to rates in the range of 10^{10}–10^{13} s^{-1}.

(vii) For not too high projectile velocities, the strain rate is proportional to the impact velocity. At larger velocities, cluster fragmentation destroys the linearity.

(viii) Due to projectile deformation, part of the stopping force is transferred to potential energy in the projectile, which indicates plastic flow in the projectile. It has a maximum shortly after maximum stopping.

Acknowledgment

E M Bringa acknowledges support from grant no. PICT2009-0092.

References

[1] Johnson R E 1990 *Energetic Charged-Particle Interactions with Atmospheres and Surfaces* (Berlin: Springer)
[2] Draine B T 2003 *Annu. Rev. Astron. Astrophys.* **41** 241
[3] Vickerman J C and Briggs D (ed) 2001 *ToF-SIMS: Surface Analysis by Mass Spectrometry* (Chichester: IM Publications)
[4] Tempez A *et al* 2004 *Rapid Commun. Mass Spectrom.* **18** 371
[5] Wucher A 2006 *Appl. Surf. Sci.* **252** 6482
[6] Winograd N 2005 *Anal. Chem.* **77** 142A
[7] Szakal C, Kozole J, Russo M F Jr, Garrison B J and Winograd N 2006 *Phys. Rev. Lett.* **96** 216104
[8] Russo M F Jr, Wojciechowski I A and Garrison B J 2006 *Appl. Surf. Sci.* **252** 6423
[9] Meiwes-Broer K H (ed) 2000 *Metal Clusters at Surfaces: Structure, Quantum Properties, Physical Chemistry (Springer Series in Cluster Physics)* (Berlin: Springer)
[10] Brown W L, Jarrold M F, McEachern R L, Sosnowski M, Takaoka G, Usui H and Yamada I 1991 *Nucl. Instrum. Methods* B **59–60** 182
[11] Haberland H, Insepov Z and Moseler M 1993 *Z. Phys.* D **26** 229
[12] Haberland H, Insepov Z and Moseler M 1995 *Phys. Rev.* B **51** 11061
[13] Perez A *et al* 1997 *J. Phys. D: Appl. Phys.* **30** 709
[14] Palmer R E, Pratontep S and Boyen H G 2003 *Nat. Mater.* **2** 443
[15] Harbich W 2000 *Metal Clusters at Surfaces: Structure, Quantum Properties, Physical Chemistry* (*Springer Series in Cluster Physics*) (Berlin: Springer) p 107
[16] Toyoda N, Hagiwara N, Matsuo J and Yamada I 2000 *Nucl. Instrum. Methods* B **161** 980
[17] Carroll S J, Nellist P D, Palmer R E, Hobday S and Smith R 2000 *Phys. Rev. Lett.* **84** 2654
[18] Anders C and Urbassek H M 2005 *Nucl. Instrum. Methods* B **228** 57–63
[19] Aoki T, Seki T, Matsuo J, Insepov Z and Yamada I 1998 *Mater. Chem. Phys.* **54** 139
[20] Anders C and Urbassek H M 2007 *Nucl. Instrum. Methods* B **258** 497–500
[21] Michels A, Wijker H and Wijker H K 1949 *Physica* **15** 627
[22] Hansen J P and Verlet L 1969 *Phys. Rev.* **184** 151
[23] Wilson W D, Haggmark L G and Biersack J P 1977 *Phys. Rev.* B **15** 2458
[24] Gades H and Urbassek H M 1995 *Phys. Rev.* B **51** 14559–69
[25] Colla T J and Urbassek H M 2000 *Nucl. Instrum. Methods* B **164–165** 687–96

[26] Ziegler J F, Biersack J P and Littmark U 1985 *The Stopping and Range of Ions in Solids* (New York: Pergamon)
[27] Beeler J R Jr 1983 *Radiation Effects Computer Experiments* (Amsterdam: North-Holland)
[28] Anders C and Urbassek H M 2007 *Phys. Rev. Lett.* **99** 027602-1-4
[29] Anders C and Urbassek H M 2008 *Nucl. Instrum. Methods* B **266** 44–8
[30] Anders C, Ziegenhain G, Zimmermann S and Urbassek H M 2009 *Nucl. Instrum. Methods* B **267** 3122–5
[31] Bringa E M, Rosolankova K, Rudd R E, Remington B A, Wark J S, Duchaineau M, Kalantar D H, Hawreliak J and Belak J 2006 *Nat. Mater.* **5** 805
[32] Ziegler J F 2000 *SRIM* http://www.srim.org/
[33] Sigmund P 1989 *J. Vac. Sci. Technol.* A **7** 585
[34] Sigmund P 1989 *J. Physique* C **50** 175
[35] Shulga V I, Vicanek M and Sigmund P 1989 *Phys. Rev.* A **39** 3360
[36] Shulga V I and Sigmund P 1990 *Nucl. Instrum. Methods* B **47** 236
[37] Sigmund P 1981 *Sputtering by Particle Bombardment I* ed R Behrisch (Berlin: Springer) p 9
[38] Meyers M A, Remington B A, Maddox B and Bringa E M 2010 *JOM* **62** 24
[39] Insepov Z, Manory R, Matsuo J and Yamada I 2000 *Phys. Rev.* B **61** 8744
[40] Preston D L, Tonks D L and Wallace D C 2003 *J. Appl. Phys.* **93** 211
[41] Quinones S A and Murr L E 1998 *Phys. Status Solidi* a **166** 763
[42] Murr L E, Quinones S A, Ferreyra E, Ayala A, Valerio O L, Hörz F and Bernhard R P 1998 *Mater. Sci. Eng.* A **256** 166